



# Oxidative dehydrogenation of *n*-octane using vanadium-magnesium oxide catalysts with different vanadium loadings

Elwathig A. Elkhalifa, Holger B. Friedrich \*

School of Chemistry, University of KwaZulu-Natal, Westville Campus, Private Bag X54001, Durban 4000, South Africa

## ARTICLE INFO

### Article history:

Received 11 September 2009  
Received in revised form 29 October 2009  
Accepted 3 November 2009  
Available online 10 November 2009

### Keywords:

Oxidative dehydrogenation  
*n*-Octane  
Styrene  
Octenes  
VMgO catalysts

## ABSTRACT

In this study, vanadium-magnesium oxide (VMgO) catalysts with different vanadium loadings were synthesized by the impregnation method and characterized by BET, ICP-OES, IR, powder XRD, TEM, SEM, TPR-H<sub>2</sub>, and TPD of ammonia. The catalysts were tested for the oxidative dehydrogenation (ODH) of *n*-octane in a continuous flow fixed bed reactor at GHSV of 6000 h<sup>-1</sup> and a temperature range of 350–550 °C using air as an oxidant and nitrogen as a make-up gas to give 9% *n*-octane in the gaseous mixture. The results showed that the vanadium concentration affects both textural and chemical properties of the catalysts and consequently their catalytic activity and selectivity towards the desired products (octenes and aromatics). The catalyst with a V<sub>2</sub>O<sub>5</sub> concentration of 15% showed the best catalytic activity and productivity for the ODH products; especially for 1-octene and styrene.

© 2009 Elsevier B.V. All rights reserved.

## 1. Introduction

Medium and long chain linear paraffins are a major byproduct of coal- and gas-to-liquids technology. With the increasing number of these plants world-wide, the supply of these low value chemicals is expected to rise rapidly and a need exists to convert these to value-added products.

The oxidative dehydrogenation (ODH) over VMgO catalysts of shorter alkanes to produce the corresponding olefins and dienes has been an active area of research [1–4]. The phase that is responsible for the ODH selectivity in the VMgO system, however, is still a topic of debate. Some attribute this selectivity to the orthovanadate [1,5–7], while others refer it to the pyrovanadate [8,9]. Also it has been suggested that the active phase is a monolayer of amorphous VO<sub>4</sub><sup>3-</sup> units scattered over MgO as isolated and polymeric species [10]. The degree of interaction between vanadium and magnesium oxide was found to affect the vanadate phases formed [11]. Therefore changing factors like vanadium loadings and/or the preparation procedure, e.g. the pH, will result in different degrees of interaction between vanadium and MgO. Consequently different proportions of the vanadate phases will be formed and ultimately affect the ODH selectivity of

the system. A noticeable feature of the VMgO system is its reluctance to form oxygenates and cracking products [3,12,13]. Thus VMgO was considered a good candidate for the ODH of higher alkanes, in this case *n*-octane, to produce the corresponding olefins and aromatics.

Dehydrogenation of *n*-octane has previously been conducted non-oxidatively [14–16], and when oxygen was employed the aim was to produce hydrogen or syngas [17,18]. Recently, we reported an oxidative dehydrogenation of *n*-octane to styrene using catalysts derived from hydrotalcite-like precursors that contain magnesium and vanadium [19]. To the best of our knowledge, no work concerning the usage of VMgO in the ODH of *n*-octane has been reported. The advantage of ODH over non-oxidative dehydrogenation is that it is thermodynamically favourable [20]. However, because of the stability of the final products, viz. H<sub>2</sub>O and CO<sub>2</sub>, controlling the reaction to intermediate stages (e.g. olefins and aromatics) is a key challenge. In this approach, influencing the residence time of the formed ODH products on the catalyst surface is likely to affect the selectivity pattern of the products. This residence time is, among other factors, a function of the phasic composition of the catalyst, as well as its surface acid–base character [1,3]. Thus vanadium concentrations may be used to influence these two properties (phasic composition and the acid–base character) without compromising the merits of the VMgO. In this work, catalysts with different vanadium loadings have been prepared and tested for the ODH of *n*-octane.

\* Corresponding author. Tel.: +27 31 2603107; fax: +27 31 2603091.  
E-mail address: [friedric@ukzn.ac.za](mailto:friedric@ukzn.ac.za) (H.B. Friedrich).

## 2. Experimental

### 2.1. Synthesis

VMgO catalysts with different vanadium loadings of 5, 15, 25 and 50%, designated 5-, 15-, 25-, 50-VMgO, have been prepared by impregnation of MgO with aqueous solutions of ammonium vanadate. The vanadium loading expresses the weight percentage of  $V_2O_5$  in the total weight of both  $V_2O_5$  and MgO. With regard to the impregnation, the procedure has some similarities with that reported in [1]. Thus, for the preparation of MgO, an aqueous solution of magnesium acetate (53.3 g in one liter) was heated to 50 °C. A hot aqueous solution of oxalic acid, which contains the exact stoichiometric amount needed to form  $MgC_2O_4$  (31.5 g in 800 ml), was added to the acetate solution and the mixture stirred for half an hour to allow for complete precipitation of the magnesium oxalate. The resultant magnesium oxalate was filtered off and the precipitate was washed thoroughly with cold and hot water and placed overnight in an oven operated at 110 °C. MgO was obtained by heating the magnesium oxalate at 600 °C for 6 h. MgO so-obtained was impregnated with a clear hot aqueous solution of  $NH_4VO_3$  (greenish yellow in colour) that contains the amount of vanadium needed for the required  $V_2O_5$  loading. As an example, for the catalyst 15-VMgO, 1.625 g of ammonium vanadate was dissolved in 750 ml of water and heated at 60 °C till the vanadate was completely dissolved. This solution was then added (while hot) to a thick paste of MgO (7.133 g) and the resultant mixture was heated, and magnetically stirred, till a paste was formed. The resultant paste was then placed overnight in an oven at 110 °C. The catalyst so-obtained was ground and calcined at 550 °C for 5 h. Temperature ramping during the calcinations was about 1.5 °/min until 550 °C was reached.

### 2.2. Characterization

The elemental composition of the catalysts was determined by inductively coupled plasma optical emission spectroscopy (ICP-OES) using an Optima 5300 DV PerkinElmer Optical Emission Spectrometer. The BET surface areas were measured by nitrogen physisorption isotherms at 77 K using the standard multipoint method (eleven points) on a micromeritics Gemini instrument. Prior to the analysis samples were degassed in a stream of nitrogen at 473 K for 24 h. The infrared spectra were recorded at room temperature using a PerkinElmer Spectrum 100 FT-IR Spectrometer fitted with a Universal ATR Sampling Accessory. A small amount of the powder catalyst was placed on top of the ATR crystal (composite of zinc selenide and diamond) and a pressure of about 120 Gauge was applied to allow for better contact between the sample and the crystal. Powder X-ray diffraction patterns were recorded on a Philips PW1050 diffractometer equipped with a graphite monochromator and operated at 40 kV and 40 mA. The source of radiation was  $Co K\alpha$ . The  $2\theta$  covers the range between 10 and 70° at a speed of one degree per minute with a step size of 0.02° and all data were captured by a Sietronics 122D automated microprocessor. Employing the peak at 50°, the average crystallite size was calculated using the Scherrer equation. The instrumental broadening on this peak was accounted for by running a standard (quartz powder) at about the same  $2\theta$ . Scanning electron microscopy (SEM) images were obtained using a LEO 1450 Scanning Electron Microscope. Samples for SEM images were coated with gold using a Polaron SC Sputter Coater. Transmission electron microscopy (TEM) images were taken on a Jeol JEM 1010 Transmission Electron Microscope operated at a voltage of 100 kV. Samples were prepared by deposition of a small amount of the catalyst between two formvar coated copper grids and the images were captured with MegaView III Soft Imaging System. Tempera-

ture-programmed reduction (TPR) and  $NH_3$ -temperature-programmed desorption (TPD) experiments were carried out in a Micromeritics 2900 AutoChem II Chemisorption Analyzer. Prior to the reduction in the TPR, the catalyst was pretreated by being heated under a stream of argon (30 ml/min) at 400 °C for 30 min and then cooled down to 80 °C under the same stream of argon. In the reduction experiment, 5%  $H_2$  in argon was used as a reducing agent at a flow rate of 50 ml/min. To account for the difference in vanadium concentrations across the catalysts, different weights were used in the analysis (18–94 mg). Under these reducing conditions, the temperature was ramped up to 950 °C at a rate of 10°/min. To investigate the resultant phase(s) of this reduction, powder XRD was carried out on catalyst samples after being reduced and the small sample size was overcome by using a blank holder. In the TPD experiments, the catalyst (ca. 20 mg) was first flushed at 350 °C with helium flowing at 20 ml/min for 30 min and the temperature was thereafter brought down to 80 °C. A 4.1% ammonia in helium gas mixture was then passed (20 ml/min) over the catalyst for 30 min. The excess ammonia was removed by flushing the system with helium (30 ml/min) for 30 min and the adsorbed ammonia was then stripped off by the same stream of helium (30 ml/min) and a temperature ramp of up to 900 °C (at 10°/min) and the desorption profiles were recorded.

### 2.3. Catalytic testing

Catalyst testing was carried out in a continuous flow fixed bed reactor (down flow mode). The reactor tube was stainless steel with an internal diameter of 10 mm and a length of 220 mm. The catalyst volume was 1 ml (ca. 0.45 g) sandwiched between two layers of glass wool and all void spaces were packed with carborandum. The catalyst pellets' sizes were between 600 and 1000  $\mu m$ . An electrically heated block, equipped with a temperature controller and a thermocouple, was used to heat the reactor tube. The temperature of the catalyst bed was monitored with a coaxially centered thermocouple placed at the middle of the catalyst bed. The concentration of *n*-octane in the gaseous mixture was 9% (v/v) and its molar ratio to oxygen was 0.8. Air was used as an oxidant and nitrogen as a make-up gas to give a total flow of 100 ml/min. *n*-Octane was delivered to the system by an HPLC pump. The liquid products and the unreacted octane were collected in a catchpot cooled to about 2 °C and the volume of the gaseous components was measured by a Ritter Drum-Type Gas Meter. The products were analyzed, off line, using a gas chromatograph (PerkinElmer Clarus500) equipped with both an FID and a TCD. The TCD was used for the analysis of carbon oxides and the FID for the rest of the products in both gaseous and liquid phase. An Agilent 6890 Series GC System equipped with an Agilent 5973 Network Mass Selective Detector was used to identify the catalytic test products, and further confirmation was done by direct injection of the identified products in the GC. Blank tests under experimental conditions indicate that the non-catalytic contribution was negligible. Carbon balances ranged from 95 to 101% and all data points were obtained in duplicate.

## 3. Results and discussion

### 3.1. Catalyst synthesis

An aqueous environment was chosen for the synthesis, though some studies have opted for organic media [21,22]. Magnesium oxide, with its isoelectric point of 11 to 12.7, forms a basic solution that will interact with the ammonium vanadate solution. Magnesium oxalate was first decomposed to magnesium oxide prior to the impregnation as it was suspected that the oxalate stabilizes the  $V^{4+}$  [23]. Before calcination all the catalysts were

**Table 1**  
Chemical composition and textural properties of VMgO catalysts.

Catalyst	Nominal wt% of V <sub>2</sub> O <sub>5</sub>	Actual wt% of V <sub>2</sub> O <sub>5</sub> (ICP)	Surface area (m <sup>2</sup> /g)	Crystallite size from XRD (nm)	Particle size from TEM (nm)
5-VMgO	5	6.46	124	7.0	7.5
15-VMgO	15	15.96	173	7.0	6.6
25-VMgO	25	26.87	79	6.4	7.0
50-VMgO	50	52.24	41	8.2	9.0
MgO	0	0	119	13.3	14.0

white and after calcination they turned yellow, with the colour intensifying as the vanadium concentration increases.

### 3.2. Characterization

As Table 1 reveals, there was no continuous trend between the vanadium concentration and the resultant surface area, but it can be noted that the incorporation of vanadium onto the magnesium oxide causes an increase in the surface area to a certain point (15%) and a noticeable decrease takes place thereafter.

#### 3.2.1. Infrared spectroscopy

As Fig. 1 displays, the infrared spectrum of the 5-VMgO showed two weak bands at around 816 and 877 cm<sup>-1</sup>. According to Sam et al. [8], the band around 877 cm<sup>-1</sup> is indicative of the orthovanadate (asymmetric stretching of the VO<sub>4</sub> group). The band at 816 cm<sup>-1</sup> is attributable to the pyrovanadate phase [1,24]. This indicates that both phases are present in the 5-VMgO. However,

the weakness of these bands implies that both phases are present in small quantities. Similarly, the band at 816 cm<sup>-1</sup> and the shoulder at around 877 cm<sup>-1</sup> in the spectrum of the 15-VMgO (Fig. 1) indicate the presence of both pyrovanadate and orthovanadate, respectively. A noticeable feature is that the presence of pyrovanadate is more manifested compared to that of the 5-VMgO catalyst. The spectrum of the 25-VMgO (Fig. 1) also shows the existence of both phases but with different vibration modes. This activation and deactivation of vibrations may probably be due to different interactions and coexistence modes between different phases as the vanadium concentration increases. With its C<sub>2v</sub> point group of symmetry, the pyrovanadate could vibrate either through the terminal VO<sub>3</sub> or the skeletal VOV bridge [25]. According to Kung and co-workers [1] and Sam et al. [8], the bands at 667 and 831 cm<sup>-1</sup> are due to the asymmetric stretching of the VOV group in the pyrovanadate and the asymmetric stretching of the VO<sub>4</sub> group in the orthovanadate, respectively. In the high vanadium loading, 50-VMgO, both pyro- and ortho-vanadate became even more manifested as shown by Fig. 1(d). The band at 663 cm<sup>-1</sup> is assignable to the asymmetric vibration of the VOV group [1,8], and that at 825 cm<sup>-1</sup> is attributable to the asymmetric vibration of the VO<sub>4</sub> group of the orthovanadate [24]. The slight shift of these two bands towards lower wave numbers implies more interaction between these phases at such high vanadium concentration. It can be inferred from the above that both pyrovanadate and orthovanadate are present in all the catalysts. Moreover, these phases are more manifested with increasing the vanadium concentration. No band attributable to V<sub>2</sub>O<sub>5</sub> was observed. In fact it has been reported that the interaction between vanadium and magnesium inhibits the formation of V<sub>2</sub>O<sub>5</sub> [26]. The

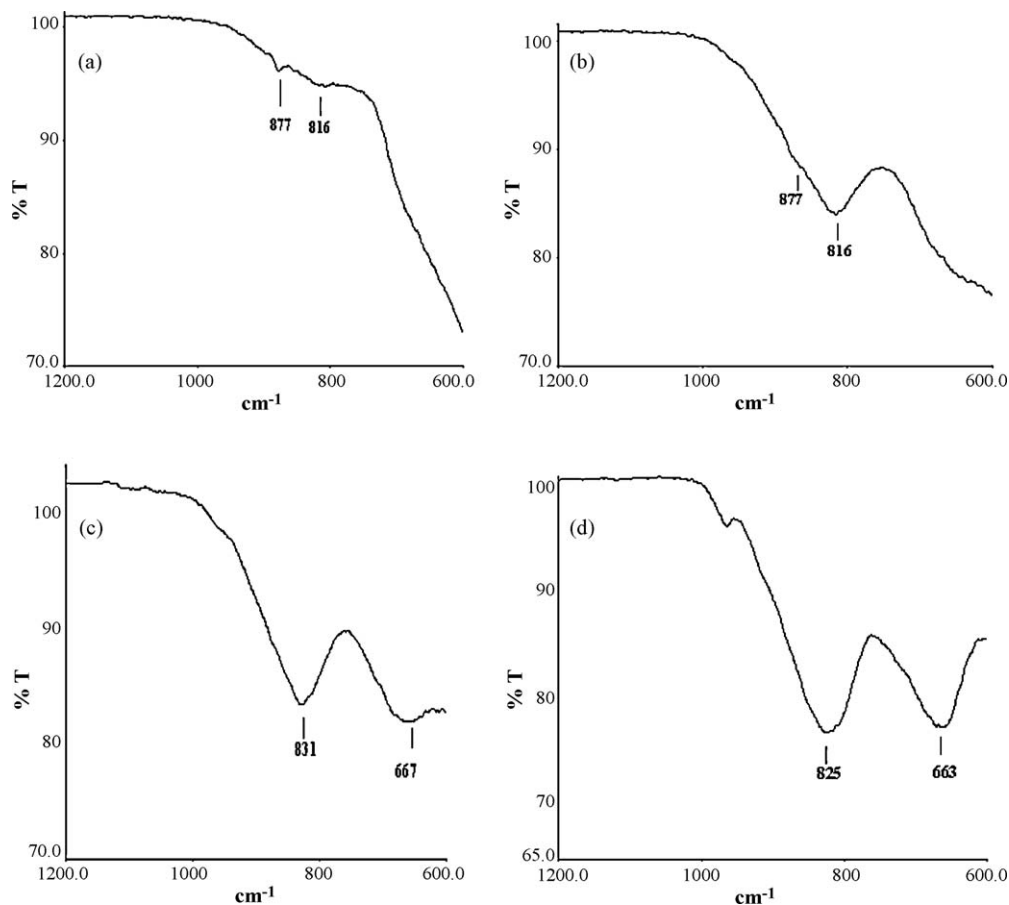


**Fig. 1.** IR spectra of (a) 5-VMgO, (b) 15-VMgO, (c) 25-VMgO, and (d) 50-VMgO.

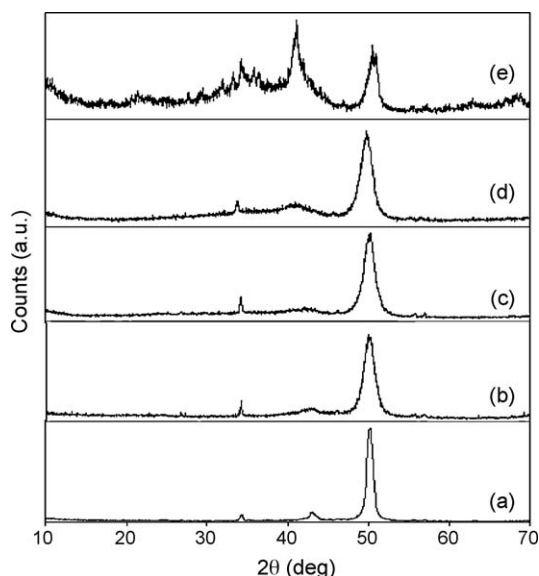


**Fig. 2.** XRD diffractograms; (a) MgO, (b) 5-VMgO, (c) 15-VMgO, (d) 25-VMgO, and (e) 50-VMgO.

exposed V=O bond in this oxide is thought to be responsible for oxygenates formation and deep oxidation that leads to the formation of  $\text{CO}_x$  [13].

### 3.2.2. Powder X-ray diffraction

Fig. 2 displays the diffraction patterns of the four catalysts, as well as magnesium oxide. The diffraction patterns of the catalysts 5-, 15-, and 25-VMgO show two lines characteristic of magnesium orthovanadate [1,27] at  $2\theta$  equal  $34^\circ$  ( $d$  spacing of 3.04 Å) and at  $42^\circ$  ( $d$  spacing of 2.5 Å). In all three catalysts no band characteristic of pyrovanadate was recorded; IR, however, showed its existence. This implies that pyrovanadate in these three catalysts is either of low concentrations or poorly crystalline and highly dispersed. In the extreme vanadium loading (50-VMgO), however, a crystalline phase of pyrovanadate was detected, along with the orthovanadate, by the lines at  $2\theta$  of  $33$  and  $36^\circ$  ( $d$  spacings of 3.12 and 2.91 Å, respectively) [27]. The diffraction patterns of all the catalysts show the existence of magnesium oxide with its characteristic line at  $2\theta$  equal  $50^\circ$  ( $d$  spacing of 2.1 Å). Again, and as shown by IR, no line attributable to  $\text{V}_2\text{O}_5$  or magnesium metavanadate was recorded.

The average crystallite sizes (Table 1) show irregular trends, though they fall within narrow limits of 6.4–8.2 nm, with the vanadium concentrations; an observation similar to this was reported by Vidal-Michel and Hohn [28]. However, a drawback of the line broadening technique is that it gives only the crystallite size in the direction perpendicular to the plane of the chosen  $2\theta$ , besides the difficulty in estimating the broadening due to the crystal deformation [29]; it is useful, therefore, to compare the sizes obtained by this technique with sizes obtained by other techniques such as TEM. The fair agreement between these average sizes and particle sizes estimated by the TEM (Table 1) implies that, in addition to the particles' uniformity, there was no significant contribution from the crystal deformation to the line broadening used for the crystallite size calculation.

### 3.2.3. Electron microscopy

As portrayed by the SEM micrographs (Fig. 3), in the pure MgO the surface displays large stacked plates and with the low vanadium concentration (5-VMgO) these plates become a bit smaller, probably by undergoing a fragmentation due to the incorporation of vanadium. In support of this is that MgO showed the highest crystallite and particle sizes and also the initial

incorporation of vanadium onto MgO caused an increase in the surface area (Table 1). When reaching a higher vanadium concentration (15-VMgO), the micrographs reflect a rough surface with relatively small platelets and the vanadium seems to be uniformly distributed over the catalyst surface. At higher vanadium concentrations, i.e. 50-VMgO and to some extent 25-VMgO, vanadium dispersion on the surface seems to be negatively affected as white particles appear, implying that vanadium starts to agglomerate on the catalyst surface. Generally, these SEM images indicate that 15-VMgO possesses the most uniform vanadium distribution on the catalyst surface. As Fig. 4 displays, the TEM micrographs of the MgO shows stacked big rounded particles. This feature is partly shown in the micrograph of the 5-VMgO indicating that the surface is only sparingly covered with vanadium. The micrographs of the 15- and 25-VMgO showed a uniform distribution of the particles, while that of 50-VMgO exhibits relatively large particles. As mentioned in Section 3.2.2, there was a good comparison between the crystallite sizes calculated by the Scherrer equation and the particle sizes estimated from the TEM micrographs as shown in Table 1.

### 3.2.4. Temperature-programmed reduction

As appears from the TPR profiles in Fig. 5, the maximum temperature for reduction increases parallel to the vanadium concentrations, indicating that total reduction becomes more difficult as the vanadium loading rises. With the exception of 5-VMgO, however, the onset temperatures are within a comparable range (Table 2). According to the assignments reported by Chang et al. [30], our XRD investigations on the reduced catalysts (Fig. 6 and Table 2) suggest, with the exception of the 5-VMgO, the formation of the spinel magnesium vanadate ( $\text{Mg}_2\text{VO}_4$ ), indicating that vanadium was predominantly reduced from  $\text{V}^{5+}$  to  $\text{V}^{4+}$ . The exception related to 5-VMgO was also reflected in its peculiar profile which shows two peaks (and a shoulder) compared to one main peak for the rest. Each of the 15- and the 25-VMgO TPR profiles show one main peak. However, the peaks' shapes, along with the hydrogen consumption and the corresponding oxidation states of the reduced vanadium (Table 2), indicate that vanadium was predominantly reduced to  $\text{V}^{4+}$  and that minor further reduction to  $\text{V}^{3+}$  was also took place. In the lowest (5-VMgO) and the highest (50-VMgO) vanadium concentrations, however, the situation was a little different, as these two catalysts showed two peaks with a shoulder and a peak with a shoulder, respectively. For the 5-VMgO, the first peak at  $590^\circ\text{C}$  and the shoulder at  $670^\circ\text{C}$  are probably due to the reduction of vanadium in slightly different environments and, as indicated by the hydrogen consumption, they are likely of the same type of reduction ( $\text{V}^{5+}$  to  $\text{V}^{4+}$ ). The second peak, however, is presumably for a further reduction step, as inferred from the hydrogen consumption and from the absence of lines attributable to the formation of  $\text{V}^{4+}$  species in the XRD of the reduced material (Table 2). The absence of the  $\text{V}^{4+}$  species in the reduced sample of this catalyst may be attributed to the further reduction of  $\text{V}^{4+}$  and to low vanadium concentration in this catalyst. In the extreme vanadium loading (50-VMgO), the main peak at  $755^\circ\text{C}$  and the shoulder at around  $825^\circ\text{C}$  indicate that vanadium is present in two different coordination environments. This is in agreement with the remark that high vanadium concentrations lead to the formation of octahedrally coordinated species in addition to the tetrahedrally coordinated ones [31]. In fact, at such high vanadium concentration, coupled with low surface area ( $41\text{ m}^2/\text{g}$ ), the presence of surface and bulk vanadium species is conceivable; the shoulder may be attributed to the reduction of the bulk vanadium species. The TPR of MgO did not show any peaks, indicating that all the observed peaks are due to the reduction of vanadium.

Considering the charge balance of the reduction  $\text{V}^{5+}$  to  $\text{V}^{4+}$ , and assuming that the same type of reduction is likely to take place

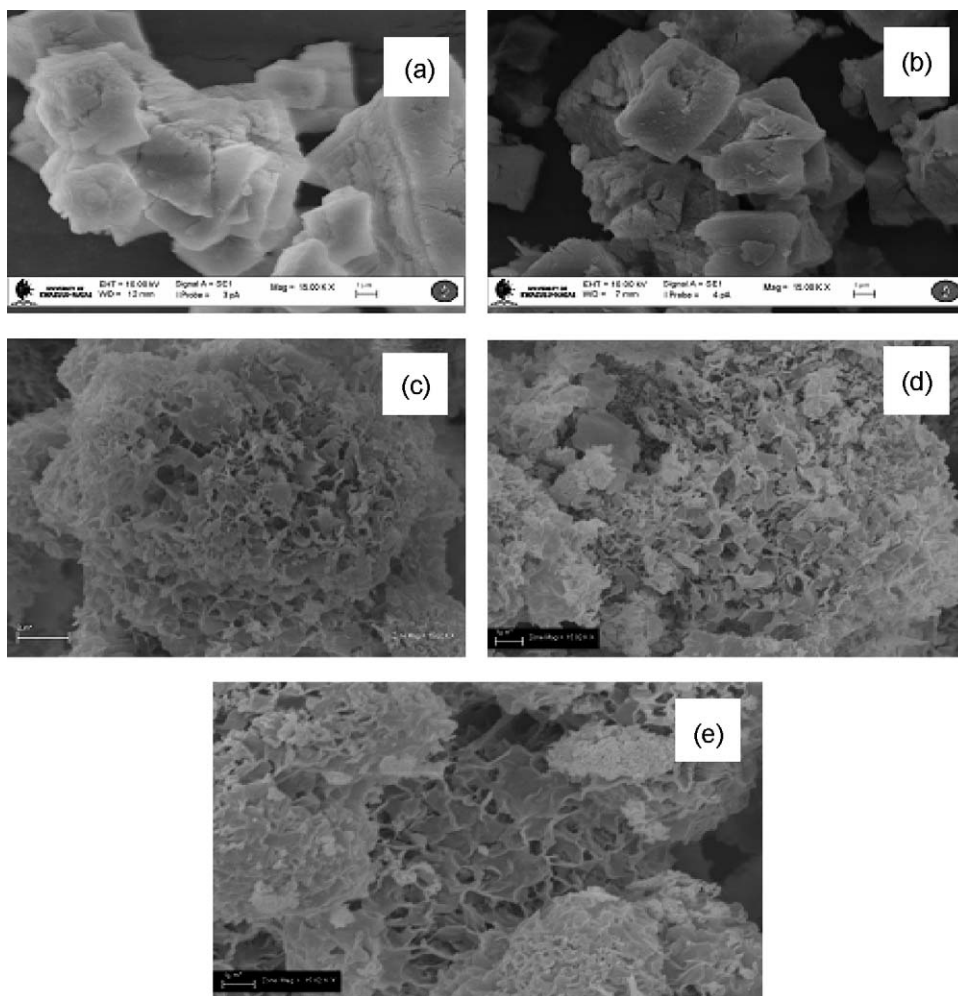


Fig. 3. SEM images (15,000 times magnification) of (a) MgO, (b) 5-VMgO, (c) 15-VMgO, (d) 25-VMgO, and (e) 50-VMgO.

during the catalyst testing, the VMgO system is likely to furnish the less nucleophilic  $O^-$  specie which is thought to enhance ODH products over oxygenates' formation [12]. In support of this is that during the testing of the catalysts reported here only traces of oxygenates were observed.

### 3.2.5. Temperature-programmed desorption

Table 3 shows that magnesium oxide, though known for its Brønsted basicity, possesses some sort of surface acidity, which is probably of a Lewis nature. Indeed, it has been reported that the MgO surface appears to show some acidity and that ammonia can be adsorbed onto the MgO surface by the interaction of its lone pair with  $Mg^{2+}$  cations [32–34]. Each of the VMgO catalysts exhibits two types of acidic sites; one around 450 °C (nominally denoted as weak acidic sites), and the other at around 650 °C (strong acidic sites). As Table 3 shows, increasing vanadium loading causes the total acidity to increase, as is the case for 5- and 15-VMgO, but with more vanadium loadings (25- and 50-VMgO) the acidity started to drop. This decrease in the acidity may be attributed to the phasic composition of the catalyst (namely the coexistence of pyro and orthovanadate) and/or the decrease of the support (MgO) contribution to the acidity as a result of the support coverage by the added vanadium.

### 3.3. Catalytic testing

The catalytic testing was carried out over the temperature range of 350–550 °C with each temperature being held for around

24 h. To investigate the catalysts' stability, the temperature was dropped down to 350 °C and ramped again to 550 °C and results very similar to the original ones were obtained. The GHSV was kept at 6000  $h^{-1}$  throughout this study which corresponds to the flow rates of 9, 54 and 37 ml/min for gaseous *n*-octane, air and nitrogen, respectively.

#### 3.3.1. Catalytic activity

Fig. 7a shows the variation of conversion with temperature for different VMgO catalysts. For all the catalysts, the conversion increases as the temperature rises. At low temperatures (350 and 400 °C), 5-VMgO shows highest catalytic activity. This activity at low temperatures (especially at 350 °C) can be attributed to the reducibility of this catalyst as reflected by its TPR profile (Fig. 5a) which exhibits an early reduction peak at around 590 °C with an onset temperature around 340 °C. However, as the temperature increases, i.e. 450 °C and above, the catalyst 15-VMgO dominates the other catalysts as it shows a noticeably higher conversion. Unlike the 5-VMgO catalyst, the other three catalysts showed very low conversion at 350 °C (around 2–3%). This is parallel to their comparable onset temperatures as shown by the TPR results (Fig. 5 and Table 2). An assessment of the oxygen conversion, Fig. 7b, indicates that the system was operating under aerobic conditions, which supports the assumption that this reaction is predominantly oxidative, as it is believed that the non-oxidative dehydrogenation over VMgO is likely to start when oxygen is totally consumed [35].

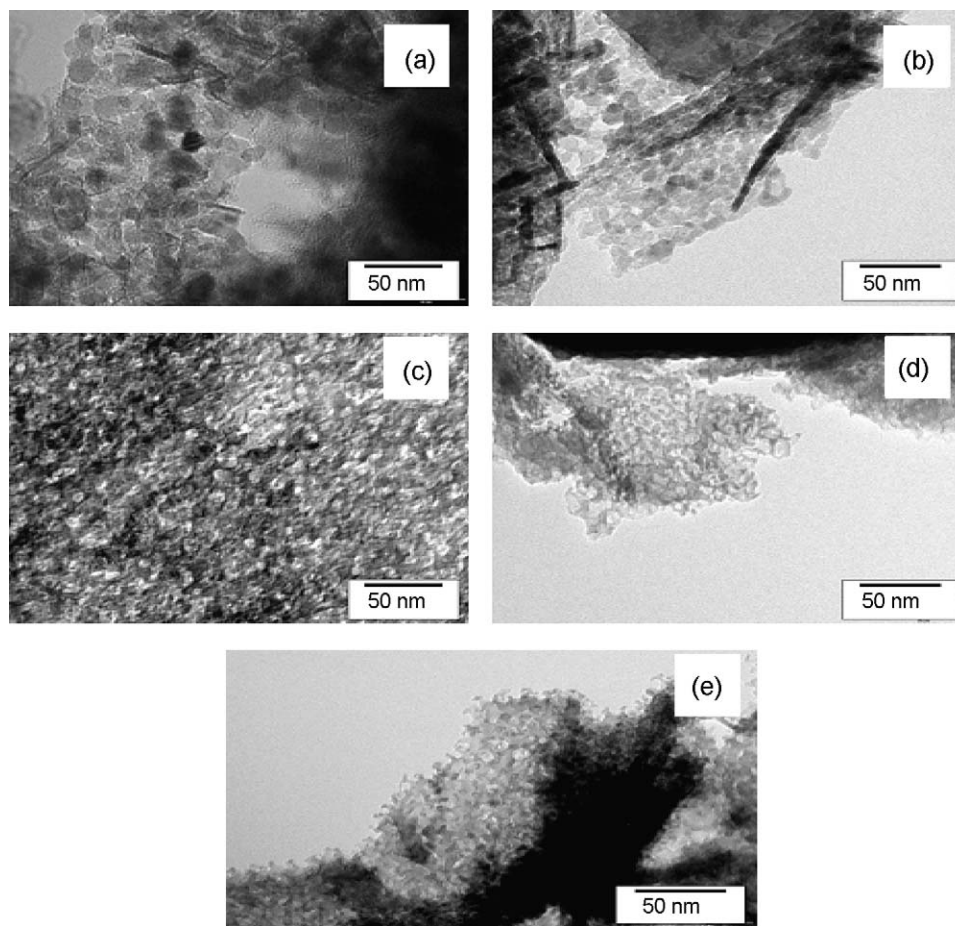


Fig. 4. TEM micrographs (500,000 times magnification) of (a) MgO, (b) 5-VMgO, (c) 15-VMgO, (d) 25-VMgO, and (e) 50-VMgO.

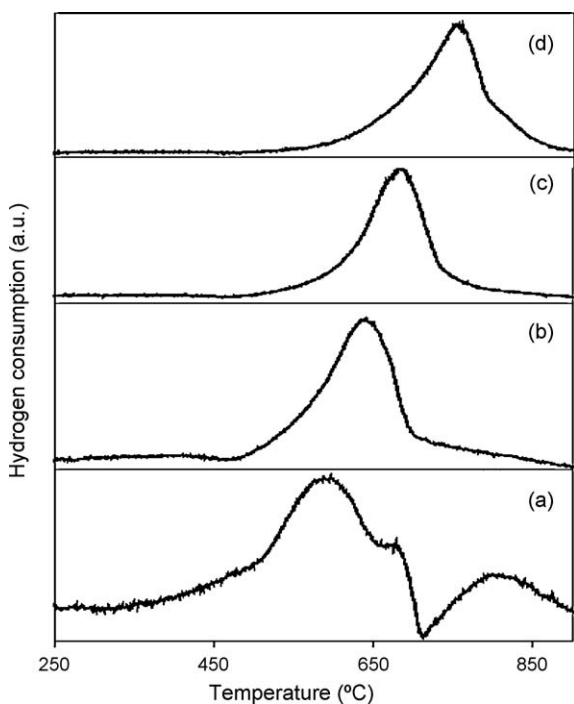


Fig. 5. TPR profiles of (a) 5-VMgO, (b) 15-VMgO, (c) 25-VMgO, and (d) 50-VMgO.

### 3.3.2. Product selectivity on VMgO catalysts

As Fig. 8a shows, octenes selectivity over the four catalysts is generally high when compared to the aromatics selectivity (Fig. 8b). This might be attributable to the basic nature of the MgO. Apparently paradoxically, at low temperatures (350–450 °C) and with the only exception of 50-VMgO at 400 °C, the octenes selectivity increases as the vanadium loading increases (i.e. as MgO concentration decreases). Alkenes selectivity in general is attributable to a short residence time on the catalysts' surface as the quick desorption minimizes the chances for further undesirable reactions, viz., cracking or secondary combustion to  $\text{CO}_x$  [1,3,11]. This short residence time on the catalyst surface at the high vanadium loading (50% and to some extent 25% vanadium loading) could either due to the acid–base character and/or to the phasic composition of the catalyst. As Table 3 reveals, the total acidity increases when moving from 5 to 15%  $\text{V}_2\text{O}_5$  nominal concentration, and as the  $\text{V}_2\text{O}_5$  concentration reaches 25 and 50%, the acidity starts to drop. This low acidity at high vanadium loadings is likely to enhance the desorption of the formed octenes, which eventually leads to a high selectivity to these compounds on the 25- and 50-VMgO catalysts. In addition to the above, the IR and XRD investigations in this study suggest that the magnesium pyrovanadate phase is manifested, along with the presence of orthovanadate, as the vanadium concentration increases. The possible synergistic coexistence between these two phases could also enhance the fast desorption of the formed octenes from the catalyst surface and thereby increase their selectivity. At high temperatures, 500 and 550 °C, this trend is somewhat disrupted, as

**Table 2**  
Summary of the peaks and the resultant phase in the TPR experiments.

Catalyst	Onset temperature	Peak 1	Peak 2	Peak 3	H <sub>2</sub> consumed (μmol/g)	Oxidation state of reduced V	XRD lines for Mg <sub>2</sub> VO <sub>4</sub> in Å <sup>a</sup>
5-VMgO	340	590	670	805	332 <sup>b</sup> and 431 <sup>c</sup>	4.0 and 3.7	–
15-VMgO	475	638	–	–	850	3.9	4.91 Å
25-VMgO	490	685	–	–	1980	3.6	4.86, 2.98, 1.62
50-VMgO	510	755	825 (shoulder)	–	4003	3.5	4.88, 2.98, 1.62

<sup>a</sup> *d*-Spacing of the lines assigned to Mg<sub>2</sub>VO<sub>4</sub> [30].

<sup>b</sup> Hydrogen consumed for the first two peaks.

<sup>c</sup> Total hydrogen consumed at the end of the TPR experiment.

the 15-VMgO showed the lowest octenes selectivity; however, 50-VMgO still maintains the highest octenes selectivity. This discontinuity in the octenes selectivity trend with vanadium concentrations is likely due to the aromatics formation at these high temperatures. In support of this is that 15-VMgO showed the highest aromatics selectivity and correspondingly the lowest octenes selectivity. The opposite was true for the 50-VMgO, as it exhibited the highest octenes selectivity and the lowest selectivity to aromatics. This suggests that octenes are precursors to the aromatics, especially at high temperatures where the provision of the energy required for this transformation is likely to be met. Interestingly, only 5-VMgO forms aromatics at 350 °C (Fig. 8b) as the other three catalysts form aromatics from 400 °C and above. This is probably because of the high reducibility (low reduction temperature) of the 5-VMgO as inferred from its TPR profile (Fig. 5a).

As shown in Fig. 9a, selectivity of CO<sub>x</sub> shows a slight decrease as the temperature rises. This is possibly due to the formation of other

products; especially the aromatics. The stable aromatic nucleus in styrene, ethylbenzene and xylene represents a driving force for the formation of these compounds and thereby reduces the production of carbon oxides, especially the contribution from secondary combustion. Consistent with this is that there was a reverse relation between aromatics and CO<sub>x</sub> selectivity as shown in Figs. 8b and 9a; 15-VMgO shows the highest aromatics selectivity increase coupled with the most noticeable decrease in CO<sub>x</sub> selectivity. The same opposing trend could also be seen for CO<sub>x</sub> and aromatics selectivity over 50-VMgO. It may be concluded from this that cyclization, which eventually leads to the aromatics formation, provides an energetically favourable pathway for the reaction, which in turn decreases the formation of carbon oxides. The cracking products (C1 to C7 alkanes and alkenes) exhibit low selectivity, around 2–3%, up to 500 °C (Fig. 9b), a steep increase, however, takes place above this temperature.

### 3.3.3. Product selectivity at isoconversion

At isoconversion at 450 °C, as Fig. 10 reveals, octenes selectivity increases, though slightly, as the vanadium concentrations increase with the 50-VMgO showing the highest selectivity and 5-VMgO the lowest. This is presumably because of quick desorption of the octenes from the catalyst surface as the vanadium concentration rises. On the other hand, C8 aromatics generally show an opposite trend to that exhibited by the octenes,

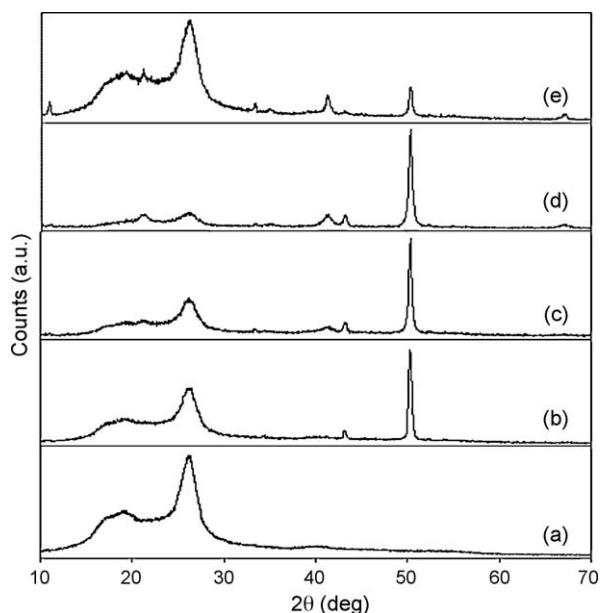


**Fig. 6.** XRD diffractograms of the reduced catalysts after TPR experiments, (a) the sample holder, (b) 5-VMgO, (c) 15-VMgO, (d) 25-VMgO, and (e) 50-VMgO.

**Table 3**  
Acidity of the different VMgO catalysts.

Catalyst	Weak acidic sites (α) (mmol NH <sub>3</sub> /g)	Strong acidic sites (β) (mmol NH <sub>3</sub> /g)	Total acidity (mmol NH <sub>3</sub> /g)
MgO	0.713	0.702	1.415
5-VMgO	1.054	0.778	1.832
15-VMgO	1.127	0.730	1.857
25-VMgO	0.911	0.880	1.790
50-VMgO	1.121	0.367	1.488

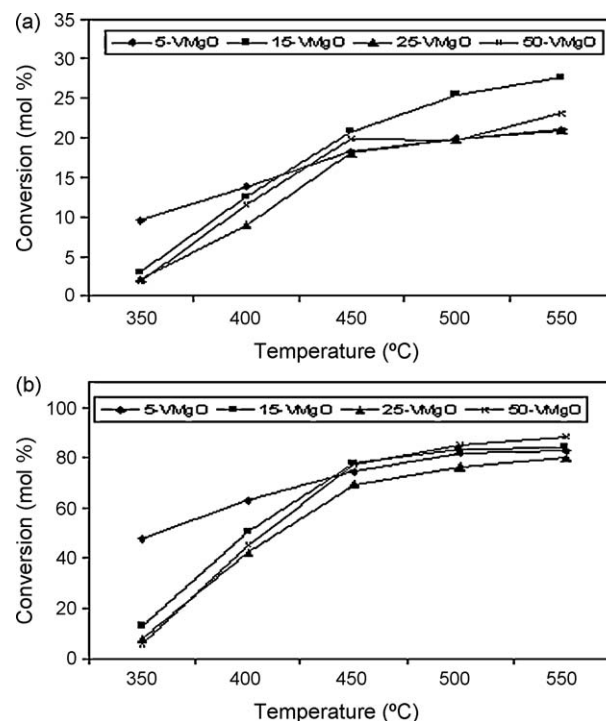


**Fig. 7.** Variation of conversion with temperature at GHSV of 6000 h<sup>-1</sup> for (a) *n*-octane (b) oxygen.

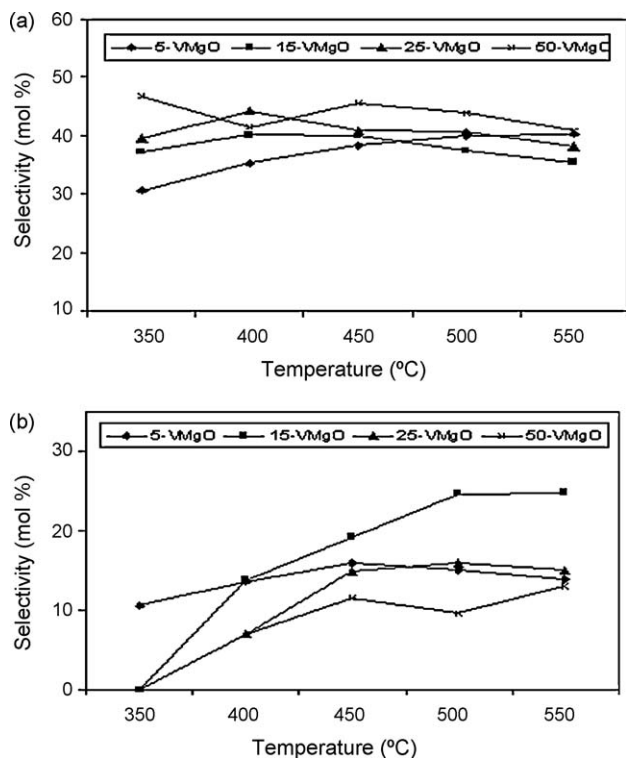


Fig. 8. Selectivity at  $6000 \text{ h}^{-1}$  for (a) octenes (b) C8 aromatics (styrene, ethylbenzene and *o*-xylene).

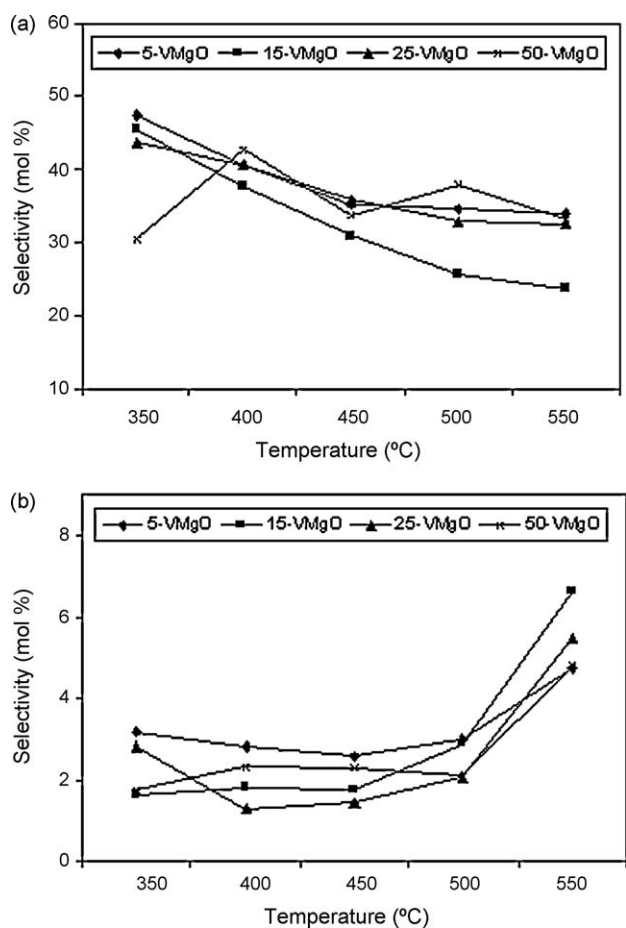


Fig. 9. Selectivity at  $6000 \text{ h}^{-1}$  for (a) CO<sub>x</sub> and (b) cracking products (C1 to C7).

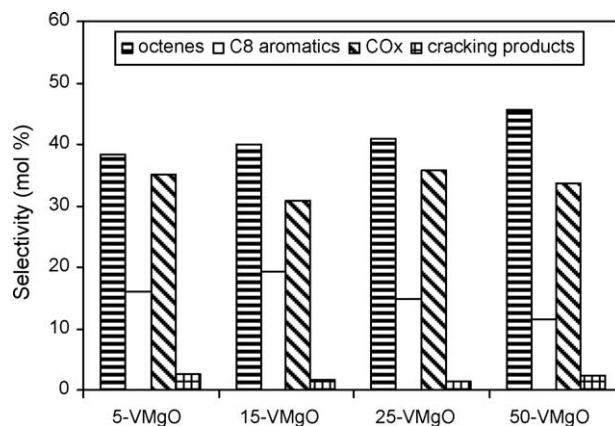


Fig. 10. Products selectivity on different catalysts at  $450 \text{ }^\circ\text{C}$  and isoconversion ( $\approx 19\%$ ).

which again suggests that octenes are aromatics precursors, and therefore fast desorption from the catalyst surface (high octenes selectivity), as is the case at high vanadium concentration (50-VMgO) will result in low aromatics selectivity. In contrast, at low vanadium loadings, 5- and 15-VMgO, a relatively slow desorption of the (basic) octenes from the catalyst surface lowers their selectivity but at the same time causes the aromatics selectivity to increase by providing more chance for the formed octenes to be oxidized further to give the corresponding aromatics, and as mentioned in Section 3.3.2. The fast (or slow) desorption of the octenes from the catalyst surface could be attributed to the acid–base character of the catalyst and/or its phasic composition. Interestingly, the selectivity to octenes and C8 aromatics at this isoconversion (19%) correlates well with both the acid–base character of the catalysts (Table 3) and their phasic composition. An interesting feature shown in Fig. 10 is that 15-VMgO showed the highest selectivity for C8 aromatics and the lowest selectivity for carbon oxides which, as mentioned in Section 3.3.2, indicates that the aromatics formation provides an energetically favourable pathway for the reaction, which in turn lowers the CO<sub>x</sub> formation. Cracking products selectivity for all the four catalysts was minimal.

At these comparative conversions (around 19%), the selectivity to the octene isomers was found to be influenced by vanadium loadings (Table 4). 15-VMgO gives the highest selectivity to 1-octene. This selectivity, however, drops as the vanadium loadings increase to 25 and 50%. 2-Octene (combined *cis* and *trans* isomers) was shown to be the dominant isomer over all four catalysts with its selectivity steadily increasing with increasing vanadium loadings. As Table 4 shows, the selectivity to *trans*-2-octene is always slightly higher than that to the *cis*-2-octene, this may be attributed to the relative thermodynamic stability of *trans* isomers in general compared to the corresponding *cis* isomers [36]. 3-Octenes, on the other hand, exhibit a noticeably higher selectivity on 50-VMgO if compared to the other three catalysts. Interestingly, 4-octenes were found to be the least produced isomers over all the catalysts, indicating that *n*-octane activation at C4 was unfavourable despite the fact that the C–H bond at this carbon is equivalent in energy to the other methylenic C–H bonds at C2 and C3 [37]. The rate-determining step in alkane activation is the homolytic rupture

Table 4  
Selectivity of the octenes at  $450 \text{ }^\circ\text{C}$  and isoconversion ( $\approx 19\%$ ).

	1-Octene	<i>trans</i> -2-octene	<i>cis</i> -2-octene	3-Octenes	4-Octenes
5-VMgO	10.8	7.3	6.3	10.5	3.5
15-VMgO	11.8	7.4	7.2	10.2	3.5
25-VMgO	11.3	8.2	7.4	10.1	3.9
50-VMgO	10.0	9.2	8.1	13.7	4.7

of the C–H bond to form the surface alkyl species, which is then followed by a fast elimination of a second hydrogen from a neighbouring carbon to form the olefinic bond [37]. However, the low selectivity to 4-octenes suggests that, beside the thermodynamic element, factors like steric effects and the number of active centers also influence the selectivity. In the activation of *n*-octane, the steric effects are likely to play a vital role as the accessibility to the active sites by such a large molecule is likely to become a limiting factor and thereby have a significant impact on the catalytic behaviour. The steric effects, besides the thermodynamic factor, can also account for the observation that 3- and 4-octenes, unlike 1-octene, are largely produced by the 50-VMgO catalyst, as the presumably high VO<sub>4</sub> density in this catalyst is likely to enhance the activation at sterically hindered positions like those of C4. Considering the alkane activation mechanism and by inspecting the relative abundance of octenes isomers (Table 4), it is plausible to assume that *n*-octane activation has occurred predominantly at C2 and C3 and to a far lesser extent at C4. Moreover, this activation is better explained by considering both the thermodynamic factors and the steric effects.

Concerning the relative abundance of the C8 aromatics (Fig. 11), styrene was constantly produced at higher selectivity, followed by ethylbenzene and then *o*-xylene. The latter shows a noticeably low selectivity over all four catalysts. A remarkable feature is that 15-VMgO shows superior styrene selectivity over the other three catalysts.

### 3.3.4. 1-Octene and styrene production

1-Octene and styrene are highly demanded products, and therefore a special focus has been given to their production. As Fig. 12a reveals, 15-VMgO is superior to the other three catalysts in 1-octene production, except at 350 °C where 5-VMgO shows the highest yield, plausibly because of its high reducibility, as indicated by its TPR profile, which allows the reaction to start at a relatively low temperature. The yield of 1-octene over the 15-VMgO shows a steady increase until 500 °C (2.6%) and a slight drop thereafter. Generally, all the catalysts showed a sharp increase in the 1-octene yield as the temperature rises from 350 to 450 °C and after that no significant change was observed. As for the case for 1-octene, 15-VMgO shows (Fig. 12b) the highest yield to styrene, showing a very sharp increase from 400 to 500 °C (1.0–3.6%). A noticeable feature shown in Fig. 12b is that 5-VMgO reaches a maximum styrene yield at 450 while 25-VMgO shows a maximum yield at 500 °C. 50-VMgO, on the other hand, shows an irregular behaviour in styrene production with temperature. The irregularity in the catalytic behaviour was a common feature for the catalyst 50-VMgO, as it appears in the octenes and C8 aromatics selectivity (Fig. 8), as well for CO<sub>x</sub> formation (Fig. 9a). This irregularity is probably related to the extremely high vanadium concentration and, as shown by the XRD,

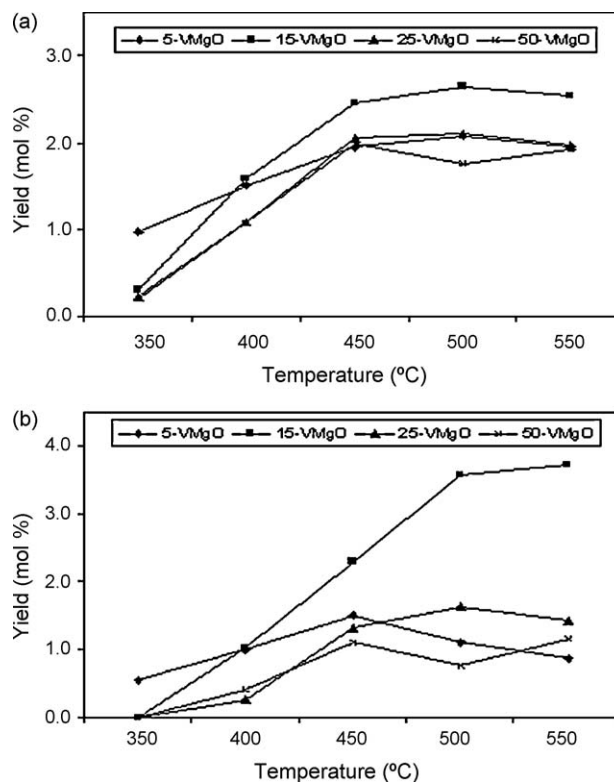


Fig. 12. The yield at 6000 h<sup>-1</sup> (a) 1-octene and (b) styrene.

that a crystalline phase of Mg<sub>2</sub>V<sub>2</sub>O<sub>7</sub> was formed only at this high concentration, along with Mg<sub>3</sub>V<sub>2</sub>O<sub>8</sub>. It was reported that magnesium pyrovanadate showed some structural instability and that during typical experimental conditions some structural changes took place [38]. In a conceivably similar behaviour, under the dynamic conditions during the catalytic testing of the 50-VMgO, some structural changes might be induced in the crystalline phase of Mg<sub>2</sub>V<sub>2</sub>O<sub>7</sub>, which in turn lead to the observed irregularity in the catalytic behaviour. In support of this is that the XRD trace of the used 50-VMgO, unlike those of the other three catalysts, was marked by the disappearance of two lines characteristic of magnesium pyrovanadate, at 2θ of 33° (*d* spacing of 3.12 Å) and 36° (*d* spacing of 2.91 Å), and moreover, a new line attributable to the pyrovanadate was observed at 2θ equal 22° (*d* spacing of 4.68 Å). This is in agreement with the observation reported in [38] that magnesium pyrovanadate undergoes structural changes during the catalyst testing. These structural changes are plausibly the cause of the irregularity observed during the catalytic testing of the 50-VMgO.

### 3.3.5. Modes of cyclization

In the case of *n*-octane, the cyclization to form a six-member carbon ring, and eventually the corresponding aromatics, could either take place via C1 to C6 or C2 to C7 bonding. The former is believed to lead to the formation of ethylcyclohexane, ethylbenzene or styrene, while the latter will result in *o*-xylene formation [39,40]. Fig. 13 shows the combined percentage of the 1–6 cyclization mode products out of the selectivity of the total cyclization products. In the ODH of *n*-octane (Fig. 13), the cyclization has taken place predominantly through the C1 to C6 mode; at low temperatures (350–450 °C) more than 90% of the cyclization follows this mode of cyclization. The tendency towards the C2 to C7 cyclization mode, however, generally increases as the temperature rises. Noticeably, the 50-VMgO catalyst showed the highest tendency towards C2 to C7 cyclization, while 15-VMgO exhibited the lowest tendency to this mode, especially between the temperatures 450 and 550 °C. It could

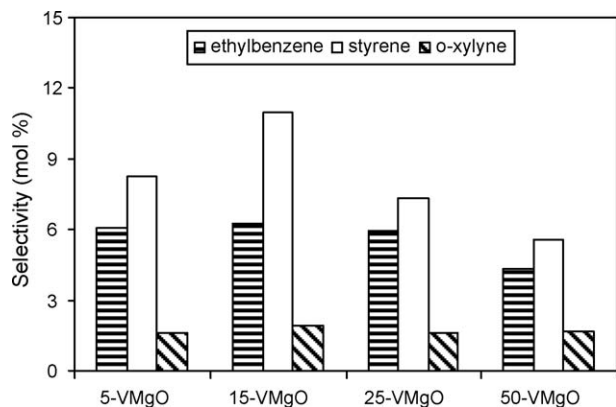


Fig. 11. Selectivity to C8 aromatics at 450 °C and isoconversion.

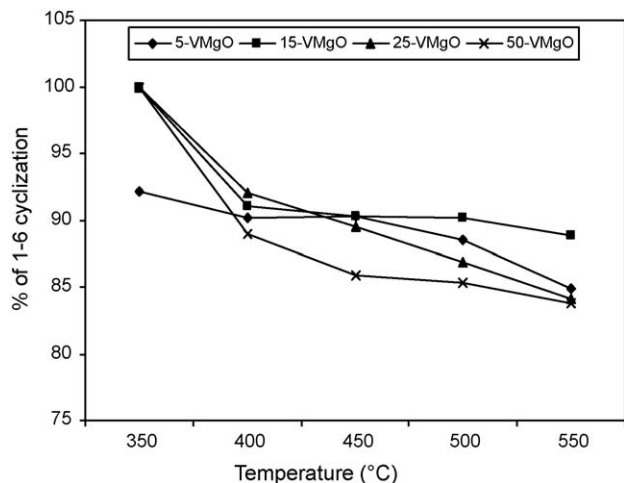


Fig. 13. The percentage of the 1–6 cyclization mode out of the total cyclization.

be concluded from the above that C1 to C6 was the favourable cyclization mode and the chance for the apparently unfavourable mode (C2 to C7) increases as the temperature rises, presumably because raising the temperature will provide more energy to overcome any activation barrier.

#### 4. Conclusions

Both textural and chemical properties of the VMgO catalysts were found to be affected by vanadium loadings. The crystalline  $\text{Mg}_3\text{V}_2\text{O}_8$  phase was formed at all vanadium loadings, while crystalline  $\text{Mg}_2\text{V}_2\text{O}_7$  was detected only at high vanadium concentration (50-VMgO); however, the formation of its amorphous form could be inferred from the IR. TPR showed that  $T_{\text{max}}$  of reduction increases as the vanadium loading increases. However, the onset temperatures of reduction were comparable, except for 5-VMgO, and they explained better the catalytic activity.

The partial oxidation of *n*-octane over VMgO catalysts produced mainly (in addition to carbon oxides) octenes, styrene, ethylbenzene and to a lesser extent xylene and some cracking products. 2-octenes were found to be the dominant octane isomers while 4-octenes were the least formed ones, indicating that *n*-octane activation was favourable at C2 and C3, and unfavourable at C4. The relative abundance of different octene isomers was found to be affected by vanadium concentration, e.g. 1-octene was the dominant isomer over 15-VMgO, while over 50-VMgO 3-octene was the dominant isomer with 1-octene being the least formed one. 50-VMgO showed the highest selectivity to the octenes and correspondingly the lowest to the aromatics. Moreover, cyclization occurred predominantly via C1 to C6 which led to the predominance of styrene and ethylbenzene over xylene.

15-VMgO was found to be superior to the other catalysts in activity as well as in the production of 1-octene and styrene.

#### Acknowledgements

We would like to thank the NRF and THRIP for support. Thanks are also extended to the Electron Microscopy Unit at the University of Kwazulu-Natal (Westville).

#### References

- [1] M.A. Chaar, D. Patel, M.C. Kung, H.H. Kung, *J. Catal.* 105 (1987) 483–498.
- [2] H.H. Kung, M.C. Kung, *Appl. Catal. A* 157 (1997) 105–116.
- [3] T. Blasco, J.M. Lopez Nieto, *Appl. Catal. A* 157 (1997) 117–142.
- [4] C. Pak, A.T. Bell, T.D. Tilley, *J. Catal.* 206 (2002) 49–59.
- [5] W. Oganowski, W. Mista, *Bull. Pol. Acad. Sci., Chem.* 32 (1984) 181–193.
- [6] M.A. Chaar, D. Patel, H.H. Kung, *J. Catal.* 109 (1988) 463–467.
- [7] W. Oganowski, J. Hanuza, L. Kepinski, W. Mista, M. Maczka, A. Wyrostek, Z. Bukowski, *J. Mol. Catal. A* 136 (1998) 91–104.
- [8] D. Siew Hew Sam, V. Soenen, J.C. Volta, *J. Catal.* 123 (1990) 417–435.
- [9] G.V. Isagulians, I.P. Belomestnykh, *Catal. Today* 100 (2005) 441–445.
- [10] A. Pantazidis, A. Burrows, C.J. Kiely, C. Mirodatos, *J. Catal.* 177 (1998) 325–334.
- [11] T. Blasco, J.M. Lopez Nieto, A. Dejoz, M.I. Vazquez, *J. Catal.* 157 (1995) 271–282.
- [12] A. Corma, J.M. Lopez Nieto, N. Paredes, *J. Catal.* 144 (1993) 425–438.
- [13] L. Balderas-Tapia, I. Hernandez-Perez, P. Schacht, I.R. Cordova, G.G. Aguilar-Rios, *Catal. Today* 107–108 (2005) 371–376.
- [14] J. Fung, I. Wang, *J. Catal.* 130 (1991) 577–587.
- [15] A. de Lucas, P. Sanchez, F. Dorado, M.J. Ramos, J.L. Valverde, *Appl. Catal. A* 294 (2005) 215–225.
- [16] A. Szechenyi, F. Solymosi, *Appl. Catal. A* 306 (2006) 149–158.
- [17] R. Subramanian, G.J. Panuccio, J.J. Krummenacher, I.C. Lee, L.D. Schmidt, *Chem. Eng. Sci.* 59 (2004) 5501–5507.
- [18] K.A. Williams, L.D. Schmidt, *Appl. Catal. A* 299 (2006) 30–45.
- [19] H.B. Friedrich, A.S. Mohamed, *Appl. Catal. A* 347 (2008) 11–22.
- [20] M.M. Bhasin, J.H. McCain, B.V. Vora, T. Imai, P.R. Pujado, *Appl. Catal. A* 221 (2001) 397–419.
- [21] L. Albaric, N. Hovnanian, A. Julbe, G. Volle, *Polyhedron* 20 (2001) 2261–2268.
- [22] I.V. Mishakov, A.A. Vedyagin, A.F. Bedilo, V.I. Zaikovskii, *Catal. Today* 144 (2009) 278–284.
- [23] A. Corma, J.M. Lopez Nieto, N. Paredes, *Appl. Catal. A* 104 (1993) 161–174.
- [24] J. Hanuza, B. Jerowska-Trzebiatowska, W. Oganowski, *J. Mol. Catal.* 29 (1985) 109–143.
- [25] K. Nakamoto, *Infrared Raman Spectra of Inorganic and Coordination Compounds*, fourth ed., John Wiley and Sons, United States of America, 1986.
- [26] L. Balderas-Tapia, J.A. Wang, I. Hernandez-Perez, G.G. Aguilar-Rios, P. Schacht, *Mater. Lett.* 58 (2004) 3034–3039.
- [27] R. Burch, E.M. Crabb, *Appl. Catal. A* 100 (1993) 111–130.
- [28] R. Vidal-Michel, K.L. Hohn, *J. Catal.* 221 (2004) 127–136.
- [29] J.R. Anderson, M. Boudart, *Catalysis Science and Technology*, 5, Springer-Verlag, Berlin, Heidelberg, 1984, pp. 221–273.
- [30] W.S. Chang, Y.Z. Chen, B.L. Yang, *Appl. Catal.* 124 (1995) 221–243.
- [31] O.R. Evans, A.T. Bell, T.D. Tilley, *J. Catal.* 226 (2004) 292–300.
- [32] S. Coluccia, E. Garrone, E. Borello, *J. Chem. Soc., Faraday Trans. 1* (79) (1983) 607–613.
- [33] S. Coluccia, S. Lavagnino, L. Marchese, *J. Chem. Soc., Faraday Trans. 1* (83) (1987) 477–486.
- [34] M. Calatayud, A. Markovits, M. Menetrey, B. Mguig, C. Minot, *Catal. Today* 85 (2003) 125–143.
- [35] N. Ballarini, A. Battisti, F. Cavani, A. Cericola, C. Cortelli, M. Ferrari, F. Trifiro, P. Arpentini, *Appl. Catal. A* 307 (2006) 148–155.
- [36] R.T. Morrison, R.N. Boyd, *Organic Chemistry*, Sixth ed., Prentice-Hall, New Jersey, 1992, pp. 317–366.
- [37] B.K. Hodnett, *Heterogeneous Catalysis Oxidation: Fundamental and Technological Aspects of the Selective and Total Oxidation of Organic Compounds*, Wiley, 2000, pp. 65–101.
- [38] S. Sugiyama, Y. Hirata, K. Nakagawa, K.-I. Sotowa, K. Maehara, Y. Himeno, W. Ninomiya, *J. Catal.* 260 (2008) 157–163.
- [39] P. Meriaudeau, A. Thangaraj, C. Naccache, S. Narayanan, *J. Catal.* 146 (1994) 579–582.
- [40] B. Shi, B.H. Davis, *J. Catal.* 157 (1995) 626–630.